



Nonlinear Dynamics Simulation Analysis of Rotor-Disc-Bearing System with Transverse Crack

Ri CholUk¹ · Zhao Qiang² · Zhang ZhunHyok¹ · Chae ChungHyok³ · Sin YongIl¹ · Ri KwangIl¹

Received: 29 March 2021 / Revised: 21 April 2021 / Accepted: 22 April 2021 / Published online: 10 May 2021
© Krishtel eMaging Solutions Private Limited 2021

Abstract

One of the main causes for failure in the rotor machine is the presence of internal cracks in the shaft rotating at high speed. The occurrence of such cracks has a dangerous and catastrophic effect on the dynamic behavior of rotating structures and can seriously affect rotating machinery. Due to the destructiveness of the cracks in rotor system, cracks were chosen as the subject of study, and the how to formulate the dynamics equation of the rotor system with and without cracks was explained. In that, the finite element analysis method was combined with the Lagrange method to concretely interpret the equation formulation. Then, the natural frequency matrix and mode of the rotor system without crack and with one crack were determined by using the ANSYS program's tetrahedral mesh and iteration strategies of Runge–Kutta. Furthermore, how the change of the crack position and the non-dimensional crack depth influence the natural frequencies of the rotor system were analyzed in detail. And, the influence of eccentricity on the rotor system and the relationship between eccentricity and nonlinearity were obtained. The result showed that when the eccentric distance and the eccentric mass were relatively small, i.e. 0.05 m, 0.001 kg, the effect on the eccentric force is almost linear, but when the eccentric distance and the eccentric mass were relatively large, i.e. 0.1 m, 0.05 kg, the nonlinear effect of eccentric forces must be considered.

Keywords Natural frequency · Rotor-disc-bearing · Transverse crack · Nonlinear dynamics · Simulation analysis

Introduction

Unlike ordinary machines, high-speed rotary machines work in harsh environments and under high stress, which results in cyclic fatigue, creep, and corrosion. All these physical phenomena lead to generation of fatigue cracks, which can severely damage machine components or even lead to catastrophic failure. In this regard, many studies have been made on rotator systems. In particular, many studies have been conducted in terms of the method of making a mathematical model of the Jeffcott rotor system and the vibration analysis method of the rotor system using the finite element

method. Many advances have been made in the establishment of the mathematical model of the Jeffcott rotor system. Zalik [1] studied the properties of the solutions of the Jeffcott equations with deadband and the method making nonlinear rotordynamics equation. Joaquín Campos et al. [2] studied a simple model capable of allowing visualization of the parameters and problematic aspects associated with a Jeffcott rotor using bond graphs. Wagner et al. [3] examined how the natural frequencies and modal damping ratios of a shaft/rotor system are affected by changes in lubricant viscosity and bearing clearance. The analysis considers a uniform elastic shaft with a single rigid rotor mounted away from mid-span and supported by fully cavitating, T-film, short-length, plain journal bearings. Yao et al. [4] introduced a concept of micro-relative displacement to describe the relative motion between each part of the planetary gear system, thus the positive semidefinite gear system is transformed into a positive definite system. By using the finite element method, the dynamic model of the whole ball bearing-rotor system is proposed by integrating the rigid body motion and the elastic vibration of the rotor [5]. A mathematical model of a lightweight flexible rotor disk bearing

✉ Zhao Qiang
cch19850101@163.com

¹ School of Mechanical Technology, Kim Chaek University of Technology, Pyongyang 950003, Democratic People's Republic of Korea

² School of Traffic and Transportation, Northeast Forestry University, Haerbin 150040, China

³ Kim Il Sung University, Pyongyang 999093, Democratic People's Republic of Korea

system with geometric eccentricity and mass imbalance was created. This mathematical model includes a bidirectional flexible shaft characterized by nonlinear curvature and gyroscopic effect, geometric eccentricity, a rigid disk crooked with unbalance mass, and nonlinear flexible bearings [6]. Lu et al. [7] formulated the kinematics equation of the system, taking into account the unbalance excitations of the two rotors, vertical constant forces acting on the rotor system and the gravities. A dynamic model of a rotor-blade system has established considering the effect of nonlinear supports at both ends, and in the proposed model, the shaft is modeled as a rotating beam where the gyroscopic effect is considered, while the shear deformation is ignored [8]. Yan et al. [9] formulated a novel fractional-order mathematical model of the rotor-bearing-seal system is established from the view of engineering applications by using the finite element method. Luo et al. [10] studied an improved transfer-matrix method (TMM) for investigating the steady-state response of complex rotor-bearing systems based on the mathematical model of the system. The method of constructing a dynamic model in a rotor system with cracks was described [11, 12]. The general contents of the nonlinear vibration, the method making the motion equation of the cracked rotor and the method of solving the nonlinear vibration were studied and analysed [13]. In the spring-mass-coupled system, the vibration analysis method and the calculation method of the critical speed were specifically mentioned [14]. In this paper, a model for the dynamics of fast rotating, elastic beams supported in hydrodynamic bearings is derived and its vibration behavior analyzed. The continuous rotor is modelled using Euler–Bernoulli beam theory under the inclusion of rotatory inertia and gyroscopic effects [15]. The natural frequency analysis and calculation method of the rotating machinery considering the gyroscopic effect, and the imbalance and balance were studied [16]. A rotordynamic analysis of a large turbocompressor that models both the casing and supports along with the rotor-bearing system was performed. A 3D finite element model of the casing captures the intricate details of the casing and support structure [17]. Bajpai et al. [18] studied of natural frequency characteristics of structural steel and alloy 6061 system composed of various material by using ANSYS program. Meshing method and modelling of a Simple 3D Cantilever Beam Using SOLID Elements is specifically mentioned [19]. In the rotary system considering the gyroscopic effect and whirl, the method of modelling and analyzing the system using the finite element method was mentioned [20]. Using ANSYS Workbench, the structure modelling, dynamic analysis, and vibration analysis method were analysed [21]. In the previous studies, the dynamic modelling and vibration analysis of the rotor system with cracks were widely discussed with many methods. In the dynamic modelling, however, no specific analysis has been made on the modelling methods of with and without cracks,

and few have been made on the basis of this model to interpret the natural frequency problems of the rotor system in the two cases of cracks and without cracks. In this paper, therefore, the method of creating the dynamic equation of the rotor system with and without cracks by using the finite element method and the Lagrange equation, the method of calculating the critical speed, and How the natural frequency of the rotor system changes according to the position of the crack and the change of the non-dimensional crack depth and influence of eccentricity on the rotor system was analyzed in detail.

Mathematical Modelling of the Rotor-Disc-Bearing System

System Equation of Motion Without Crack

Motion Equation of Element

The rotor system is generally composed of a rigid disk, a rotor shaft, and a bearing. Their motion equations will be established respectively and further assembled to form the entire system equation (Fig. 1).

Motion Equation of Shaft Element Figure 2 is an elastic axial segment whose local nodes are numbered as 1 and 2.

The generalized coordinate of this element is the displacement of the nodes at both ends, that is:

$$\begin{cases} \{u_{1z}\} = [x_A, \theta_{yA}, x_B, \theta_{yB}]^T \\ \{u_{2z}\} = [y_A, -\theta_{xA}, y_B, -\theta_{xB}]^T \end{cases} \quad (1)$$

In any section within the element, the displacement x, θ_y, y, θ_x is a function of position s and time t . By using the displacement interpolation function and the displacement of the node of the element, the displacement x, θ_y, y, θ_x can be expressed as:

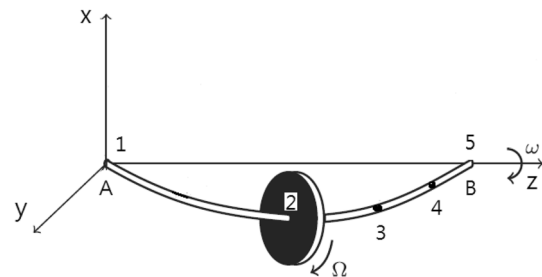


Fig.1 Rotor-disc-bearing system

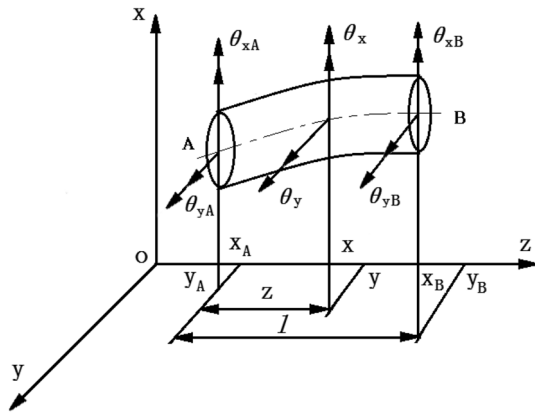


Fig.2 Elastic axial segment

$$\begin{cases} x(s, t) = [N] \{u_{1s}\} \\ y(s, t) = [N] \{u_{2s}\} \\ \theta_y = [N'] \{u_{1s}\} \\ -\theta_x = [N'] \{u_{2s}\} \end{cases} \quad (2)$$

where $[N]$ is the undetermined displacement interpolation function matrix or shape function matrix.

$$[N] = [N_1(z), N_2(z), N_3(z), N_4(z)] \quad (3)$$

Substituting Eq. (3) into the first term and the second term of Eq. (2) is as follows:

$$\begin{cases} x(z, t) = N_1(z)x_A(t) + N_2(z)\theta_{yA}(t) + N_3(z)x_B(t) + N_4(z)\theta_{yB}(t) \\ \theta_y(z, t) = \frac{\partial x}{\partial z} = N'_1(z)x_A(t) + N'_2(z)\theta_{yA}(t) + N'_3(z)x_B(t) + N'_4(z)\theta_{yB}(t) \end{cases} \quad (4)$$

where $N'_i(i=1, 2, 3, 4)$ is the derivative of the function with respect to z .

The endpoint conditions of the axial segment element are as follows:

$$\begin{cases} x(0, t) = x_A(t) \\ x(l, t) = x_B(t) \\ x'(0, t) = \theta_{yA}(t) \\ x'(l, t) = \theta_{yB}(t) \end{cases} \quad (5)$$

From Eq. (4) and (5), each interpolation function should be as follows:

$$\begin{cases} N_1(0) = 1; N'_1(0) = 0; N_1(l) = 0; N'_1(l) = 0 \\ N_2(0) = 0; N'_2(0) = 1; N_2(l) = 0; N'_2(l) = 0 \\ N_3(0) = 0; N'_3(0) = 0; N_3(l) = 1; N'_3(l) = 0 \\ N_4(0) = 0; N'_4(0) = 0; N_4(l) = 0; N'_4(l) = 1 \end{cases} \quad (6)$$

Because each interpolation function has four endpoint conditions, it can be assumed to be a cubic polynomial of z .

$$N_{1z} = a_0 + a_1z + a_2z^2 + a_3z^3 \quad (7)$$

Substituting Eq. (7) into Eq. (6), the constant $a_i(i=1, 2, 3, 4)$ can be determined below.

$$N_1(z) = 1 - 3\left(\frac{z}{l}\right)^2 + 2\left(\frac{z}{l}\right)^3$$

$$N_2(z) = l\left[\frac{z}{l} - 2\left(\frac{z}{l}\right)^2 + \left(\frac{z}{l}\right)^3\right]$$

$$N_3(z) = 3\left(\frac{z}{l}\right)^2 - 2\left(\frac{z}{l}\right)^3$$

$$N_4(z) = l\left[-\left(\frac{z}{l}\right)^2 + \left(\frac{z}{l}\right)^3\right]$$

For shaft segment with axisymmetric cross-sections, similarly:

$$y(z, t) = [N] \{u_{2z}\} \quad (8)$$

Based on the above results:

$$\begin{cases} x = [N] \{u_{1z}\}; \theta_y = \frac{\partial x}{\partial z} = [N'] \{u_{1z}\} \\ y = [N] \{u_{2z}\}; -\theta_x = \frac{\partial y}{\partial z} = [N'] \{u_{2z}\} \end{cases} \quad (9)$$

The kinetic energy and flexural elastic potential energy of the element can also be expressed as the function of node displacement and node velocity.

$$\begin{aligned} dT_z = & \frac{1}{2} \begin{Bmatrix} \dot{x} \\ \dot{y} \end{Bmatrix}^T \begin{bmatrix} \mu & 0 \\ 0 & \mu \end{bmatrix} \begin{Bmatrix} \dot{x} \\ \dot{y} \end{Bmatrix} dz \\ & + \frac{1}{2} \begin{Bmatrix} \theta_y \\ -\theta_x \end{Bmatrix} \begin{bmatrix} j_d & 0 \\ 0 & j_d \end{bmatrix} \begin{Bmatrix} \dot{\theta}_y \\ -\dot{\theta}_x \end{Bmatrix} \\ & + \Omega \begin{Bmatrix} \dot{x} \\ \dot{\theta}_y \end{Bmatrix}^T \begin{bmatrix} 0 & 0 \\ 0 & j_p \end{bmatrix} \begin{Bmatrix} y \\ -\theta_x \end{Bmatrix} dz \\ & + \frac{1}{2} j_p \Omega^2 dz \end{aligned} \quad (10)$$

Taking the derivative of Eq. (6) with respect to time and substituting it into for Eq. (10) is as follows:

$$\begin{aligned} dT_z = & \frac{1}{2} \{\dot{u}_{1z}\}^T \left(\mu [N]^T [N] + j_d [N']^T [N'] \right) \{\dot{u}_{1z}\} dz \\ & + \frac{1}{2} \{\dot{u}_{2z}\}^T \left(\mu [N]^T [N] + j_d [N']^T [N'] \right) \{\dot{u}_{2z}\} dz \\ & + j_p \Omega \{\dot{u}_{1z}\}^T [N']^T [N'] \{U_{2z}\} dz + \frac{1}{2} j_p \Omega^2 dz \end{aligned} \quad (11)$$

where z is the axial distance of nodal point A. The thickness of a microelement is dz , and u , j_d and j_p represent the mass, diameter, and pole moment of inertia per unit length of the axial segment, respectively. Ω is the rotational speed.

The elastic potential energy of the microelement is:

$$\begin{aligned}
 dV_z &= \frac{1}{2}EI \left\{ \begin{matrix} x'' \\ y'' \end{matrix} \right\}^T \left\{ \begin{matrix} x'' \\ y'' \end{matrix} \right\} dz \\
 &= \frac{1}{2} \left(\{u_{1z}\}^T [N'']^T [N''] \{u_{1z}\} \right. \\
 &\quad \left. + \{u_{2z}\}^T [N'']^T [N''] \{u_{2z}\} \right) \tag{12}
 \end{aligned}$$

For the circular section shaft with long l and radius r , the kinetic energy and potential energy of the element can be obtained by integrating the above two formulas along the full length of the element.

$$\begin{aligned}
 T_z &= \frac{1}{2} \{ \dot{u}_{1z} \}^T ([M_{zT}] + [M_{zR}]) \{ \dot{u}_{1z} \} \\
 &\quad + \frac{1}{2} \{ \dot{u}_{2z} \}^T ([M_{zT}] + [M_{zR}]) \{ \dot{u}_{2z} \} \\
 &\quad + \Omega \{ \dot{u}_{1z} \}^T [J_z] \{ u_{2z} \} + \frac{1}{2} J_{pz} \Omega^2 \tag{13}
 \end{aligned}$$

$$V_z = \frac{1}{2} \{ u_{1z} \}^T [K_z] \{ u_{1z} \} + \frac{1}{2} \{ u_{2z} \}^T [K_z] \{ u_{2z} \} \tag{14}$$

where

$$J_{pz} = j_{pz} l$$

$$[M_{zT}] = \int_0^l \mu [N]^T [N] dz [M_{zT}] : \textit{element's moving inertia matrix}$$

$$[M_{zR}] = \int_0^l j_d [N']^T [N'] dz \quad [M_{zR}] : \textit{rotational inertia matrix}$$

$$[G_z] = \Omega [J_z] : [G_z] : \textit{rotation matrix},$$

$$[J_z] = \int_0^l j_p [N']^T [N'] dz$$

$$[K_z] = \int_0^l EI [N'']^T [N''] dz [K_z] : \textit{stiffness matrix},$$

The motion equation of the axial segment element can be obtained from the Lagrange equation.

$$\begin{cases} [M_z] \{ \dot{u}_{1z} \} + \Omega [J_z] \{ \dot{u}_{2z} \} + [K_z] \{ u_{1z} \} = \{ Q_{1z} \} \\ [M_z] \{ \dot{u}_{2z} \} - \Omega [J_z] \{ \dot{u}_{1z} \} + [K_z] \{ u_{2z} \} = \{ Q_{2z} \} \end{cases} \tag{15}$$

where Q_{1z}, Q_{2z} correspond to the generalized force.

M_z is sum of $[M_{zT}]$ and $[M_{zR}]$

The Equation of Motion of a Rigid Disk Suppose the mass of the rigid disk, the axial area moment of inertia, and the polar moment of inertia are $m, J_d,$ and J_p respectively, and the generalized coordinate of the rigid disk is expressed

by the displacement vectors of the axis node, which are $\{u_{1d}\} = [x, \theta_y]^T$ and $\{u_{2d}\} = [y, -\theta_x]^T$, respectively.

Assuming that the disk axis coincides with the center of gravity, its kinetic energy is expressed as Eq. 16:

$$T_d = \frac{1}{2} \left\{ \begin{matrix} \dot{x} \\ \dot{y} \end{matrix} \right\}^T \begin{bmatrix} m & 0 \\ 0 & m \end{bmatrix} \left\{ \begin{matrix} \dot{x} \\ \dot{y} \end{matrix} \right\} + \frac{1}{2} \begin{bmatrix} \omega_\xi \\ \omega_\eta \\ \omega_\zeta \end{bmatrix}^T \begin{bmatrix} J_d & 0 & 0 \\ 0 & J_d & 0 \\ 0 & 0 & J_p \end{bmatrix} \begin{bmatrix} \omega_\xi \\ \omega_\eta \\ \omega_\zeta \end{bmatrix} \tag{16}$$

where $\xi\eta\zeta$ takes the axis node as origin, ξ is perpendicular to the disk plane, and the moving coordinate system fixed on the disk is shown in Fig. 3.

For θ_ξ is equal to θ_x , so

$$\begin{bmatrix} \omega_\xi \\ \omega_\eta \\ \omega_\zeta \end{bmatrix} = [A_\varphi] \begin{bmatrix} \omega_{\xi 1} \\ \omega_{\eta 1} \\ \omega_{\zeta 1} \end{bmatrix} = \begin{bmatrix} \omega_{\xi 1} \cos \varphi + \omega_{\eta 1} \sin \varphi \\ -\omega_{\xi 1} \sin \varphi + \omega_{\eta 1} \cos \varphi \\ \omega_{\zeta 1} \end{bmatrix}$$

where

$$\begin{bmatrix} \omega_\xi \\ \omega_\eta \\ \omega_\zeta \end{bmatrix} = \begin{bmatrix} \cos \varphi & \cos \theta_x \sin \varphi & 0 \\ -\sin \varphi & \cos \theta_x \cos \varphi & 0 \\ 0 & -\sin \theta_x & 1 \end{bmatrix} \begin{bmatrix} \dot{\theta}_x \\ \dot{\theta}_y \\ \varphi \end{bmatrix} \tag{17}$$

where $\theta_x, \dot{\theta}_x$ and $\dot{\theta}_y$ are all first-order microelement, and φ is equal to Ω . Substitute Eq. (17) into Eq. (16), and omit microelement higher than the second order, and consequently, following equation comes out:

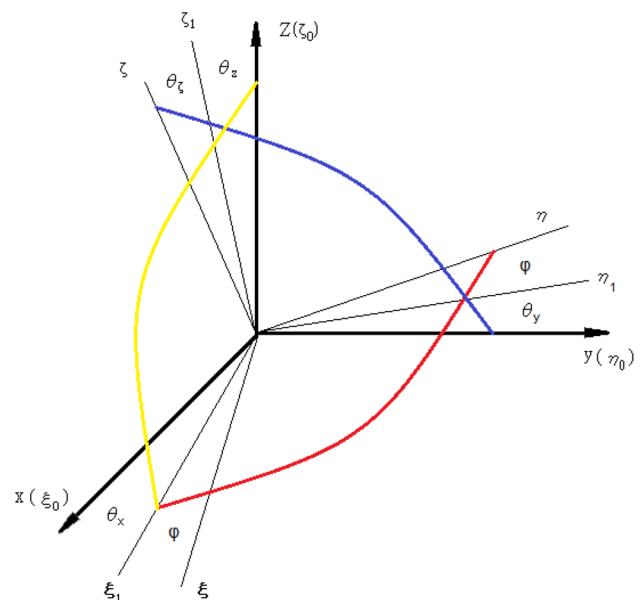


Fig.3 Motion coordinate system fixed on the rigid disk

$$T_d = \frac{1}{2} \{ \dot{u}_{1d} \}^T [M_d] \{ \dot{u}_{1d} \} + \frac{1}{2} \{ \dot{u}_{2d} \}^T [M_d] \{ \dot{u}_{2d} \} + \Omega \{ \dot{u}_{1d} \}^T [J] \{ \dot{u}_{2d} \} + \frac{1}{2} J_p \Omega^2 \tag{18}$$

where

$$[M_d] = \begin{bmatrix} m & 0 \\ 0 & J_d \end{bmatrix}, [J] = \begin{bmatrix} 0 & 0 \\ 0 & J_p \end{bmatrix}$$

The motion equation of the disk element can be obtained from the Lagrange equation:

$$\begin{cases} [M_d] \{ \ddot{u}_{1d} \} + \Omega [J] \{ \ddot{u}_{2d} \} = \{ Q_{1d} \} \\ [M_d] \{ \ddot{u}_{2d} \} - \Omega [J] \{ \ddot{u}_{1d} \} = \{ Q_{2d} \} \end{cases} \tag{19}$$

where $[M_d]$ is the mass matrix of the disk; $[G_d] = \Omega [J]$ is the rotation matrix; $\{ Q_{1d} \}$ and $\{ Q_{2d} \}$ are the corresponding generalized forces.

The Equation of Motion of a Bearing Takes a sliding bearing as bearing. For example, under the condition of good foundation rigidity, the bearing seat can be simplified into a mass-spring-damper model which is an anisotropic bearing model as shown in Fig. 4.

The corresponding dynamic characteristic coefficient matrix is as below:

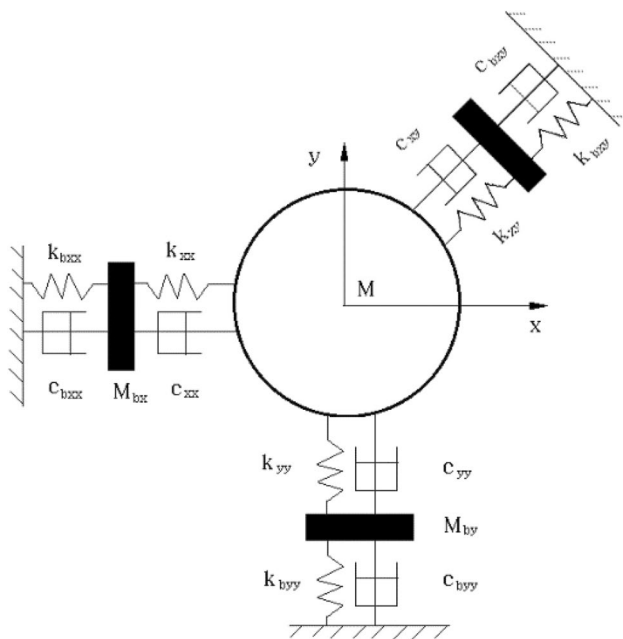


Fig.4 Mass-spring-damper model

$$[C_b] = \begin{bmatrix} c_{bxx} & c_{bxy} \\ c_{byx} & c_{byy} \end{bmatrix} [K_b] = \begin{bmatrix} K_{bxx} & K_{bxy} \\ K_{byx} & K_{byy} \end{bmatrix}$$

The dynamic characteristic coefficient matrix comprehensively reflects the damping and stiffness characteristics of the bearing pedestal and foundation. The equivalent mass of bearing pedestal and foundation in x and y directions is expressed by M_{bx} and M_{by} respectively. On the supposition that the coordinate of the bearing center is x_b, y_b and the number of the corresponding journal center node is $z(j)$ and the coordinate of the journal center is $x_{z(j)}$ and $y_{z(j)}$, the motion equation of the bearing is shown below:

$$\begin{bmatrix} M_{bx} & 0 \\ 0 & M_{by} \end{bmatrix} \begin{Bmatrix} \ddot{x}_b \\ \ddot{y}_b \end{Bmatrix} + \begin{bmatrix} c_{xx} & c_{xy} \\ c_{yx} & c_{yy} \end{bmatrix} \begin{Bmatrix} \dot{x}_b - \dot{x}_{z(j)} \\ \dot{y}_b - \dot{y}_{z(j)} \end{Bmatrix} + \begin{bmatrix} k_{xx} & k_{xy} \\ k_{yx} & k_{yy} \end{bmatrix} \begin{Bmatrix} x_b - x_{z(j)} \\ y_b - y_{z(j)} \end{Bmatrix} + \begin{bmatrix} c_{bxx} & c_{bxy} \\ c_{byx} & c_{byy} \end{bmatrix} \begin{Bmatrix} \dot{x}_b \\ \dot{y}_b \end{Bmatrix} + \begin{bmatrix} K_{bxx} & K_{bxy} \\ K_{byx} & K_{byy} \end{bmatrix} \begin{Bmatrix} x_b \\ y_b \end{Bmatrix} = \{ 0 \} \tag{20}$$

If the foundation rigidity is good, that is, x_b and y_b is 0, then the generalized force of the oil film acting on the center of the journal is:

$$\begin{Bmatrix} Q_{1d}^b \\ Q_{2d}^b \end{Bmatrix} = - \begin{bmatrix} c_{xx} & c_{xy} \\ c_{yx} & c_{yy} \end{bmatrix} \begin{Bmatrix} \dot{x}_{z(j)} \\ \dot{y}_{z(j)} \end{Bmatrix} - \begin{bmatrix} k_{xx} & k_{xy} \\ k_{yx} & k_{yy} \end{bmatrix} \begin{Bmatrix} x_{z(j)} \\ y_{z(j)} \end{Bmatrix} \tag{21}$$

If damping is excluded, and the coefficient can be simplified to an elastic bearing with equal stiffness where the rigidity coefficient is K_x and k_y , respectively, then

$$\begin{Bmatrix} Q_{1d}^b \\ Q_{2d}^b \end{Bmatrix} = - \begin{bmatrix} k_x & 0 \\ 0 & k_y \end{bmatrix} \begin{Bmatrix} x_{z(j)} \\ y_{z(j)} \end{Bmatrix} \tag{22}$$

Equation of Motion of the Systems

For the rotor system connected by n nodes and n-1 axial segments, the displacement vector is:

$$\begin{cases} \{ U_1 \} = [x_1, \theta_{y1}, x_2, \theta_{y2}, \dots, x_n, \theta_{yn}] \\ \{ U_2 \} = [y_1, -\theta_{x1}, y_2, -\theta_{x2}, \dots, y_n, -\theta_{xn}] \end{cases} \tag{23}$$

By synthesizing the motion equations of the disc, shaft segment and bearing, the motion equation of the system can be obtained as follows:

$$\begin{cases} [M_1] \{ \ddot{U}_1 \} + \Omega [J_1] \{ \ddot{U}_2 \} + [k_1] \{ U_1 \} = \{ Q_1 \} \\ [M_1] \{ \ddot{U}_2 \} - \Omega [J_1] \{ \ddot{U}_1 \} + [k_1] \{ U_2 \} = \{ Q_2 \} \end{cases} \tag{24}$$

where $[M_1]$ is the global mass matrix, $\Omega [J_1]$ is the rotation matrix, and $[K_1]$ is the stiffness matrix.

System Equation of Motion Having Crack

When the rotor cracks, the opening and closing behavior caused by rotor rotation and shaft selection results in time-varying stiffness. This is called a breathing crack. The dynamic equation formulation of systems with cracks must be further examined in the stiffness when has the crack. The general dynamics equation is as follows:

$$M\ddot{U} + C\dot{U} + KU = Q \tag{25}$$

where M and K are the mass and stiffness matrices of the rotor without crack.

Q means the balance and gravitational forces.

The equations of the rotor with crack can be written as

$$M\ddot{U} + C\dot{U} + (K - K_c(t))U = Q \tag{26}$$

It may be noted that the global stiffness matrix of the rotor consists of a constant component K and a time-dependent component $k_c = f(t)k_{crack}$.

k_{crack} is the crack-related stiffness matrix. The $f(t)$ function represents the breathing effect. The proportion of the crack face that is subject to tensile axial stresses will be a determining factor for the extent of crack opening. Based on assumption that the gravity force is much greater than the imbalance force, the breathing crack [3, 4] may be described as

$$f(t) = \frac{1 - \cos(\Omega t)}{2} \tag{27}$$

where Ω is the rotational speed of the rotor. As shown in Fig. 5, for $f(t) = 0$, the crack is totally closed and the rotor with crack stiffness is equal to the rotor stiffness without crack. For $f(t) = 1$, the crack is full open. A transverse crack

in a rotor shaft can be represented by the reduction of the second moment of area ΔI of the element at the location of the crack. By using Rayleigh’s method, the change in ΔI can be represented as follows:

$$\frac{\Delta I/I_0}{1 - \Delta I/I_0} = \frac{R}{l} (1 - \nu^2) F(\mu) \tag{28}$$

where I_0 , ν , μ , R , l , and $F(\mu)$ represent the second moment of area, the Poisson’s ratio, the non-dimensional crack depth, the shaft radius, the length of the section, and the compliance functions varied with the non-dimensional crack depth μ , respectively. The non-dimensional crack depth μ is given by $\mu = h/R$, where h defines the crack depth of the shaft as shown in Fig. 5.

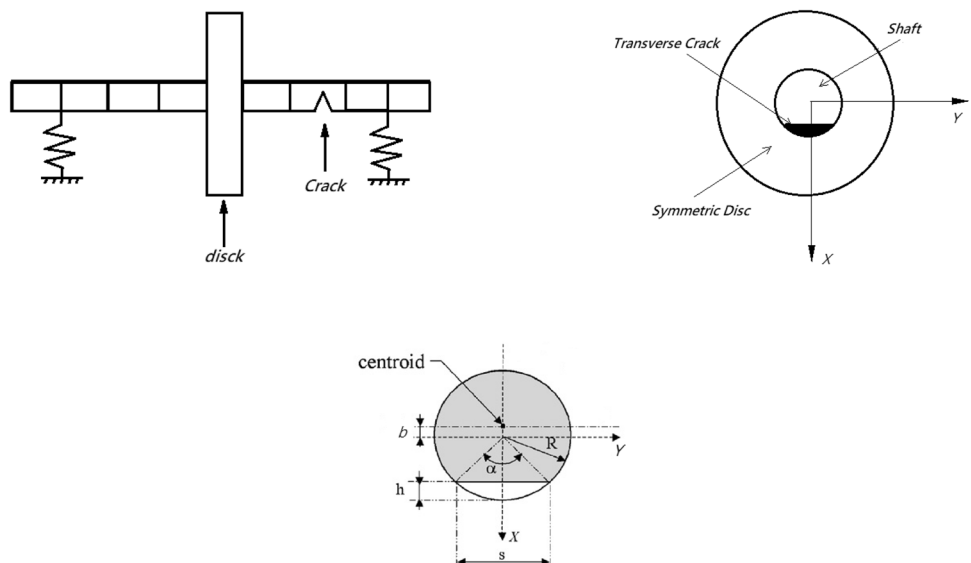
k_{crack} is given by [3, 4].

$$K_{crack} = \frac{E}{l^3} \begin{bmatrix} 12I_X & 0 & 0 & 6I_X & -12I_X & 0 & 0 & 6I_X \\ & 12I_Y & -6I_Y & 0 & 0 & -12I_Y & -6I_Y & 0 \\ & & 4I^2I_Y & 0 & 0 & 6I_Y & 2I^2I_Y & 0 \\ & & & 4I^2I_X & -6I_X & 0 & 0 & 2I^2I_X \\ & & & & 12I_X & 0 & 0 & -6I_X \\ & & & & & 12I_Y & 6I_Y & 0 \\ & Sym & & & & & 4I^2I_Y & 0 \\ & & & & & & & 4I^2I_X \end{bmatrix} \tag{29}$$

where

$$I_X = \iint Y^2 dA = \iint Y^2 dXdY = \frac{R^2}{4} \left(\delta(1 - 4\mu + 2\mu^2)\gamma + \frac{\alpha}{2} \right)$$

Fig.5 Geometric relative positions of the shaft and transverse crack



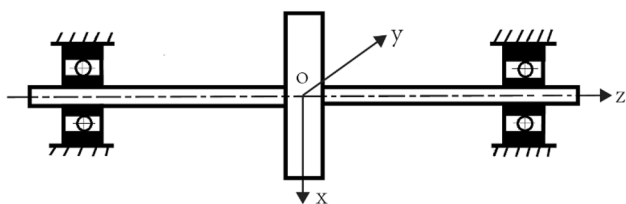


Fig. 6 Dynamic model of the rotor-disc-bearing system

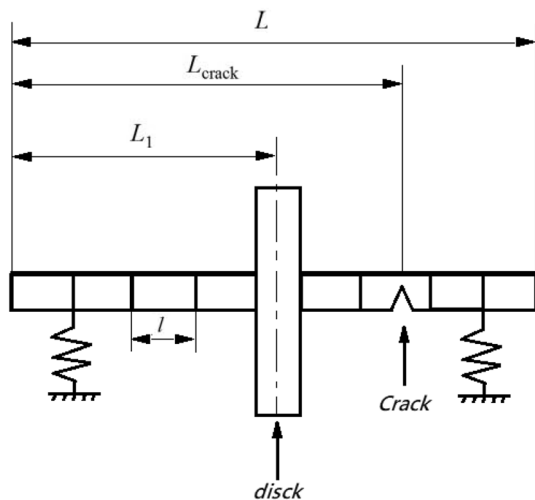


Fig. 7 Geometric model of the rotor-disc-bearing system

$$\begin{aligned}
 I_Y &= \iint X^2 dA - Ab^2 = \iint X^2 dXdY \\
 &- \left[R^2 \left(\delta\gamma + \frac{\alpha}{2} \right) \right] \left(\frac{2}{3A} R^3 \gamma^3 \right)^2 = \frac{\pi R^4}{4} \\
 &+ R^4 \left(\frac{2}{3} \delta\gamma^3 + \frac{1}{4} \delta(1 - 4\mu + 2\mu^2) \gamma + \sin^{-1} \gamma \right) \\
 &- \frac{4R^4 \gamma^6}{9 \left(\delta\gamma + \frac{\alpha}{2} \right)}
 \end{aligned}$$

where b and A are the centroid of the cross-section and the uncracked area of the cross-section, respectively, and the distance from the axis X to the centroid of the cross-section b are given by:

$$A = R^2 \left(\delta\gamma + \frac{\alpha}{2} \right)$$

$$b = \frac{2}{3A} R^3 \gamma^3$$

$$\alpha = 2\cos^{(-1)} \delta; \quad \alpha : \text{the crack angle}$$

Table 1 Parameters of the rotor system

Parameters of the rotor	Value
Young’s modulus of elasticity E , 10^{11} Pa	2.1
Density ρ , kg/m^3	7800
Poisson’s ratio μ	0.3
Axis diameter d , m	0.019
Disk diameter D , m	0.153
Thickness of disc, m	0.025
Length of the shaft L , m	1.28
Position of disc L_1 , m	0.64
Non-dimensional crack depth μ	1
Mass unbalance	0.005 g
Eccentricity of the mass m_e , kg	0.0025
Phase unbalance, degree	0
Location of the crack L_{crack} , m	0.35

Table 2 Geometric dimensions of the bearing

Parameters of the bearing	Value
External race radius r , mm	22.8
Ball diameter d , mm	13.2
Ball number N_b	7
External race mass m_w , kg	0.08
Contact stiffness K_b , $\text{N/m}^{3/2}$	11.67×10^9
Bearing clearance γ , mm	0

$$\gamma = (2\mu - \mu^2)^{0.5}$$

$$\delta = 1 - \mu$$

Nonlinear Analysis in a Rotor Disc-Bearing System by FEA

Geometric Modeling and Parameters

Geometric Modeling

Figure 6 shows the dynamic model of the rotor-disc-bearing system, which consists of a disc, a bearing and a rotating shaft. Figure 7 shows the geometric model of the rotor-disc-bearing system with crack and its geometric position relationship.

Fig. 8 Flow chart of ANSYS Simulation on Rotor System

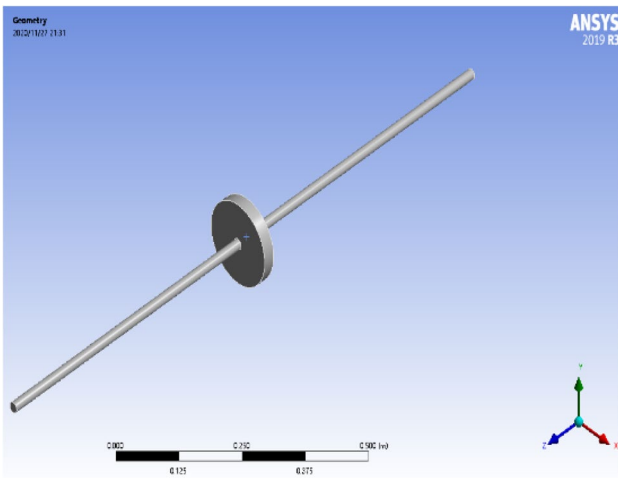
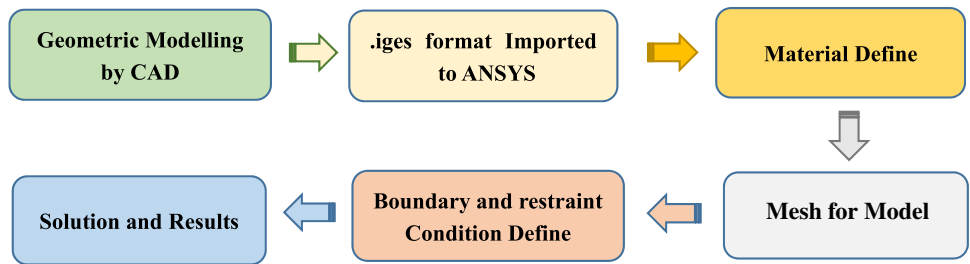


Fig. 9 Rotor System Model of without Crack

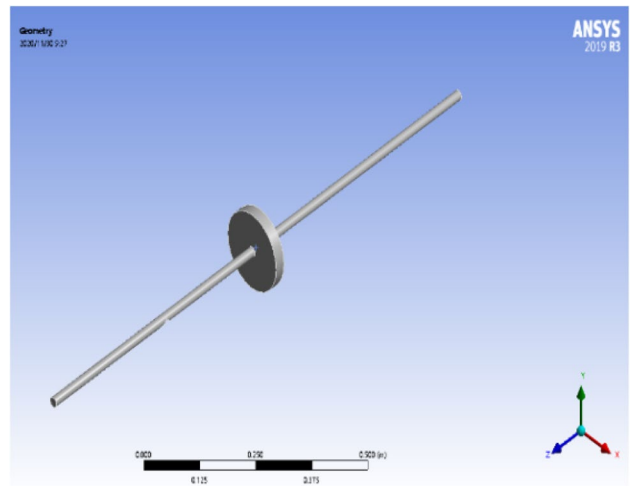


Fig.11 Rotor System Model of with Crack

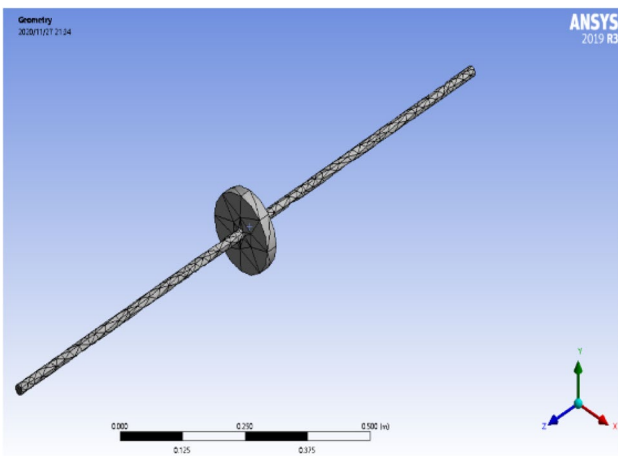


Fig.10 Rotor System Meshing of without Crack

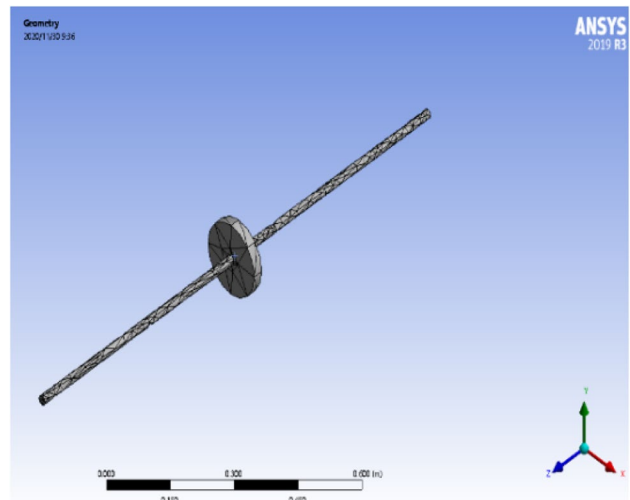


Fig.12 Rotor System Meshing of with Crack

Parameters of the Rotor System

The geometric dimension relations of rotor-disc-bearing-system and bearing are respectively shown in Table 1 and Table 2.

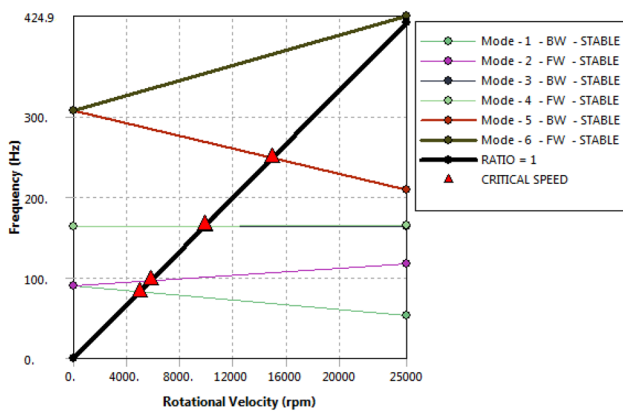


Fig.13 Result of Campbell diagrams without Crack

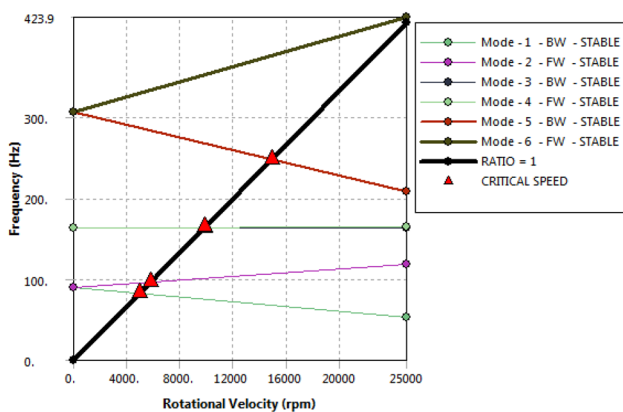


Fig.14 Result of Campbell diagrams with Crack

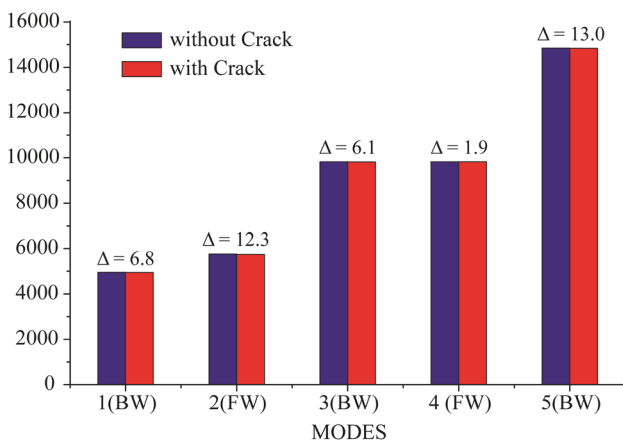


Fig.15 Graph showing Critical Speed of Rotor System without Crack and with Crack (Present). *Δ is the difference between the two values with and without cracks

Table 3 Critical speed of rotor system without crack and with crack critical speed

Modes	Without crack (present)	Without crack (Bajpai [18])	With crack (Present)	With crack (Bajpai [18])
1(BW)	4948.3	4947.5	4941.5	4957.7
2(FW)	5758.8	5768.2	5746.5	5784.3
3(BW)	9818.6	9811.2	9812.5	9855.6
4(FW)	9825.6	9829	9823.7	9880.6
5(BW)	14,849	14,855	14,836	14,927
6(FW)	None	None	None	None

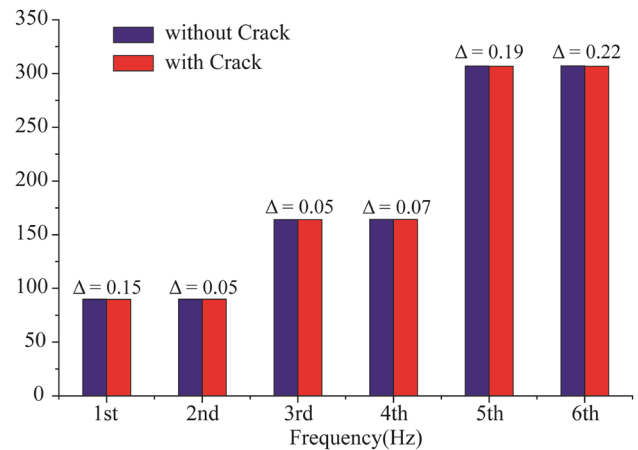


Fig.16 Graph showing the Natural frequencies of Rotor System without Crack and with Crack (Present). *Δ is the difference between the two values with and without cracks

Modelling by ANSYS

Modelling Methodology

The simulated flow chart of the rotor system using ANSYS is shown in Fig. 8.

Modelling and Mesh using ANSYS

Rotor System Model and Meshing of Without Crack The model and meshing of the rotor system without Crack using ANSYS are shown in Figs. 9 and 10.

Rotor System Model and Meshing of with Crack The model and meshing of the rotor system with Crack using ANSYS are shown in Figs. 11 and 12.

Table 4 Natural frequencies of rotor system without crack and with crack

Natural frequencies	Without crack (present)	Without crack (Bajpai [18])	With crack (Present)	With crack (Bajpai [18])
1st frequency (Hz)	89.882	89.672	89.732	89.845
2nd frequency (Hz)	89.892	89.678	89.842	89.907
3rd frequency (Hz)	164.213	163.630	164.162	164.340
4th frequency (Hz)	164.325	163.710	164.256	164.590
5th frequency (Hz)	307.024	306.000	306.825	307.480
6th frequency (Hz)	307.129	306.170	306.908	308.020

Table 5 Influence of position of the crack on the natural frequencies (the non-dimensional crack depth $\mu = 1$)

	Without crack	Position of the crack L_{crack}			
		0.25 m	0.5 m	0.75 m	0.95 m
1st frequency (Hz)	89.882	89.745	89.323	89.726	89.821
2nd frequency (Hz)	89.892	89.852	89.834	89.843	89.875
3rd frequency (Hz)	164.213	163.512	164.192	163.897	164.182
4th frequency (Hz)	164.325	164.153	164.316	164.089	164.318
5th frequency (Hz)	307.024	306.719	306.847	306.659	306.925
6th frequency (Hz)	307.129	307.082	306.912	307.115	307.119

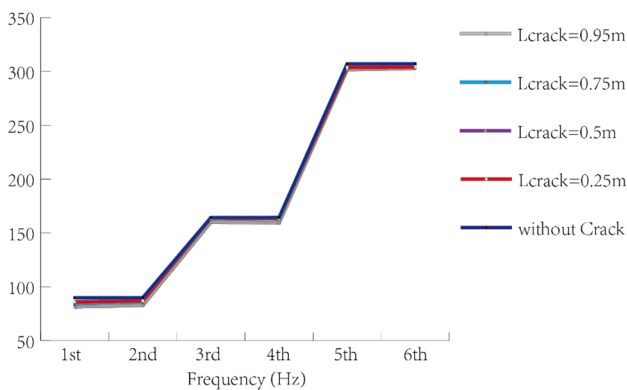


Fig.17 Graph showing the influence of the position of the crack on the natural frequencies when the non-dimensional crack depth(μ) is 1

Simulation Results

Critical Speed Analysis of Shaft Without Crack and with Crack

A modal—analysis was investigated the critical speed of shaft with crack and without crack by exploitation Campbell diagram (Figs. 13, 14 and 15).

The above table and graph shows the calculation results of the critical speed on the bearing-disc-rotor system with and without crack, and the result value is different from each other.

Considering identical material properties, disc specifications and geometrical parameters the obtained results are compared with those of Bajpai [18] as shown in Table 3. An excellent agreement could be observed in Table 3 with the results thus validating the critical speed analysis of the rotor system without crack and with crack.

Natural Frequencies Without Crack and with Crack

The above table and graph shows the calculation results of the natural frequency on the bearing-disc-rotor system with and without crack, and the result value is different from each other (Fig. 16).

Considering identical material properties, disc specifications and geometrical parameters the obtained results are compared with those of Bajpai A [18] as shown in Table 4. An excellent agreement could be observed in Table 4 with the results thus validating the natural frequencies analysis of the rotor system without crack and with crack.

Influence of non-Dimensional Crack Depth and Position of the Crack on the Critical Speed

Influence of Position of the Crack on the Natural Frequencies Table 5 and Fig. 17 show that the value of the natural frequency differs from each other according to the position of the crack as a result of the comparison of the natural frequency of the bearing-disc-rotor system that follows the position of the crack with the natural frequency value when there is no crack.

Influence of Non-dimensional Crack Depth on the Natural Frequencies Table 6 and Fig. 18 show that the contrast analysis result with the natural frequency value when there was no crack differed according to the non-dimensional crack depth with the length of the crack fixed, the change in

Table 6 Influence of non-dimensional crack depth on the natural frequencies ($L_{crack} = 0.35m$)

	Without crack	Non-dimensional crack depth μ			
		0.25	0.5	0.75	1.0
1st frequency (Hz)	89.882	89.845	89.523	89.321	89.121
2nd frequency (Hz)	89.892	89.848	89.835	89.828	89.775
3rd frequency (Hz)	164.213	164.151	164.055	163.788	162.985
4th frequency (Hz)	164.325	164.182	164.146	164.109	164.083
5th frequency (Hz)	307.024	307.012	306.953	306.879	306.695
6th frequency (Hz)	307.129	307.101	307.094	307.065	307.042

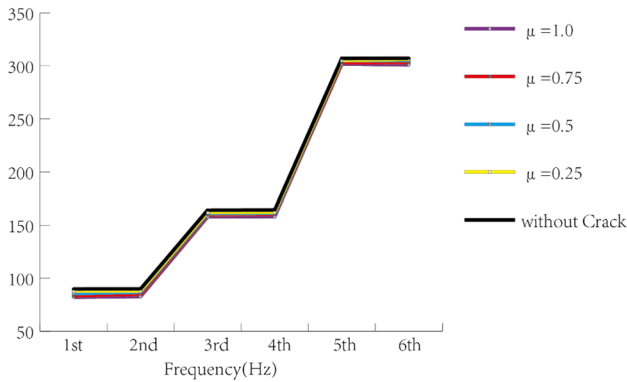


Fig.18 Graph showing the influence of non-dimensional crack depth on the natural frequencies when the Position of the crack is $L_{crack} = 0.35m$

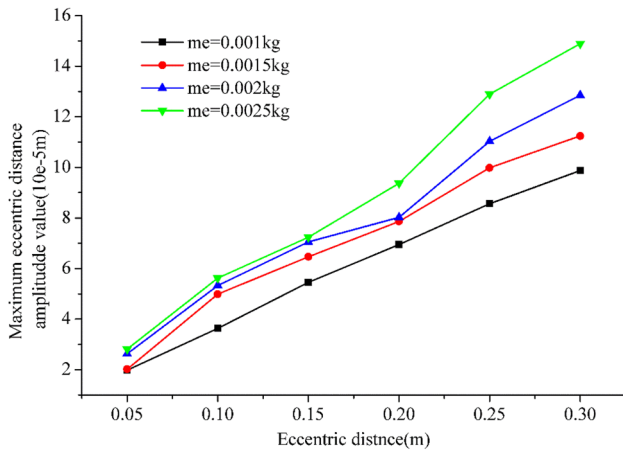


Fig.19 Vibration amplitudes relationship of disk core under different eccentric distances and eccentric masses

Table 7 Disc center vibration amplitude under different eccentric masses ($m_e=0.001$ kg)

Eccentric Distance (m)	0.05	0.1	0.15	0.2	0.25	0.3
Maximum eccentric Distance amplitude value($\times 10^{-5}$ m)	1.9851	3.6328	5.4564	6.9531	8.8629	9.8759

the natural frequency of the bearing-disc-rotor system followed by the change in the non-dimensional crack depth.

Influence Analysis of Eccentricity on the Rotor System

The important factors affecting the eccentricity of the rotor system are eccentric mass and eccentric distance. Using ANSYS program, the relation between eccentricity and non-linearity was analyzed concretely by changing eccentricity distance and eccentricity mass when the rotation number was 10000 rpm. The simulation was performed with the eccentric distance changed from 0.05 m to 0.3 m and the eccentric mass from 0.001 kg to 0.0025 kg (Table 7).

It can be seen from Tables 8, 9, 10 and Fig. 19 that the variation of the maximum amplitude when the eccentric mass is changed from 0.0025 kg to 0.001 kg is studied. The smaller the eccentric mass is, that is, the less than 0.001 kg, the effect of the eccentric mass on the rotor system is almost linear. Thus, in the eccentric rotor system, the eccentric distance and the eccentric mass are very important factors.

Discussion

As shown in the above results, the calculation results of the critical speed and natural frequency of the bearing-disc-rotor system differed with that of crack and no crack. At this time, the critical speed and natural frequency of the shaft for the crack were slightly smaller than that for no crack. Under fixation of the non-dimensional crack depth at $\mu = 1$, the natural frequency of the rotor system was analyzed by varying the position of the crack as 0.25 m, 0.5 m, 0.75 m, and 0.95 m. The natural frequency gradually decreased at the crack near 0.5 m, and then increased slightly passing 0.5 m, however, all values were smaller than the natural frequency at no

Table 8 Disc center vibration amplitude under different eccentric masses ($m_e=0.0015$ kg)

Eccentric Distance (m)	0.05	0.1	0.15	0.2	0.25	0.3
Maximum eccentric Distance amplitude value($\times 10^{-5}$ m)	2.0198	4.9865	6.4652	7.8671	9.9828	11.2432

Table 9 Disc center vibration amplitude under different eccentric masses ($m_e=0.002$ kg)

Eccentric Distance (m)	0.05	0.1	0.15	0.2	0.25	0.3
Maximum eccentric Distance amplitude value($\times 10^{-5}$ m)	2.6324	5.3258	7.0521	8.0241	11.0321	12.8542

Table 10 Disc center vibration amplitude under different eccentric distances ($m_e=0.0025$ kg)

Eccentric Distance (m)	0.05	0.1	0.15	0.2	0.25	0.3
Maximum eccentric Distance amplitude value($\times 10^{-5}$ m)	2.8125	5.6253	7.2356	9.3692	12.8965	14.8914

crack. In addition, when the position of the crack was fixed at $L_{crack} = 0.35m$, natural frequency of the shaft was analyzed changing the non-dimensional crack depth as 0.25, 0.5, 0.75, and 1.0. As the non-dimensional crack depth increased, the natural frequency gradually decreased. It can be seen from Table 8,9,10 and Fig. 19 that the variation of the maximum amplitude when the eccentric mass is changed from 0.0025 kg to 0.001 kg is studied. The smaller the eccentric mass is, that is, the less than 0.001 kg, the effect of the eccentric mass on the rotor system is almost linear. Thus, in the eccentric rotor system, the eccentric distance and the eccentric mass are very important factors. If the eccentricity distance and the eccentricity mass are small, that is, under the condition of the eccentricity distance is less than 0.05 m and the eccentricity mass is 0.001 kg, the influence of the eccentricity force on the subsystem is approximately linear. And the value of the eccentricity factor is very large, that is, in the eccentricity distance is greater than 0.3 m, the mass of the eccentricity is greater than 0.0025 kg, we should consider the nonlinear effect of the eccentricity force.

Conclusion

In this paper, how to write the dynamic equation of the rotor-disc-bearing system with and without crack was mentioned in detail combining the finite element analysis method with Lagrange method. In addition, the critical speed and natural frequency of the rotor system with and without crack were calculated using the ANSYS program. After that, how the non-dimensional crack depth and the position of the crack affect the change of the natural frequency of the rotor system was analyzed. In the analysis, the position of the crack and the non-dimensional crack depth were changed for studying the relationship between these factors and the natural

frequency of the rotor system. The natural frequency of the rotor system involving two factors was smaller than that of the uncracked system. By using ANSYS software, the influence of eccentricity on the rotor system and the relationship between eccentricity and nonlinearity were obtained. The result showed that when the eccentric distance and the eccentric mass were relatively small, i.e. 0.05 m, 0.001 kg, the effect on the eccentric force is almost linear, but when the eccentric distance and the eccentric mass were relatively large, i.e. 0.1 m, 0.05 kg, the nonlinear effect of eccentric forces must be considered.

References

- Zalik RA (1987) The Jeffcott equations in nonlinear rotordynamics. *Q Appl Math* 47(4):585–599
- Campos J, Crawford M, Longoria R (2005) Rotordynamic modeling using bond graphs: modeling the Jeffcott rotor. *IEEE Trans Magn* 41(1):274–280
- Wagner BB, Ginsberg JH (2003) Modeling the effect of bearing properties on the eigenvalues of a rotordynamic system. *J Acoust Soc Am* 113(4):2227–2227
- Yao HL, Liu Y, Ren ZH et al (2015) Research on dynamic modeling and analysis of the coupled planetary gear and rotor system. Springer International Publishing, Berlin
- Li Y, Cao H, Niu L et al (2015) A general method for the dynamic modeling of ball bearing-rotor systems. *J Manufacturing Sci Eng Transact ASME* 137(2):021016
- Phadatare HP, Pratiher B (2020) Nonlinear modeling, dynamics, and chaos in a large deflection model of a rotor-disk-bearing system under geometric eccentricity and mass unbalance. *Acta Mech* 231(3):907–928
- Lu Z, Wang X, Hou L et al (2019) Nonlinear response analysis for an aero engine dual-rotor system coupled by the inter-shaft bearing. *Arch Appl Mech* 89(7):1275–1288
- Li B, Ma H, Yu X et al (2019) Nonlinear vibration and dynamic stability analysis of rotor-blade system with nonlinear supports. *Arch Appl Mech* 89(7):1–28

9. Yan D, Wang W, Chen Q (2020) Fractional-order modeling and nonlinear dynamic analyses of the rotor-bearing-seal system. *Chaos, Solitons Fractals* 133:109640
10. Luo Z, Bian Z, Zhu Y et al (2020) An improved transfer-matrix method on steady-state response analysis of the complex rotor-bearing system. *Nonlinear Dyn* 102(1):1–13
11. Patel TH, Darpe AK (2008) Influence of crack breathing model on nonlinear dynamics of a cracked rotor. *J Sound Vib* 311(3–5):953–972
12. Rakheja S, Khorrani H et al (2017) Vibration behavior of a two-crack shaft in a rotor disc-bearing system. *Mech Machine Theory* 113:67–84
13. Ishida Y, Yamamoto T. Linear and nonlinear rotordynamics (A Modern Treatment with Applications) // Introduction. 2012, <https://doi.org/10.1002/9783527651894:1-10>.
14. J Vance, Zeidan F, Murphy B. Machinery vibration and rotordynamics (vance/machinery vibration) // Index. 2010:393–402.
15. J Rübél. Vibrations in nonlinear rotordynamics - modelling, simulation, and analysis. Philosophy, 2009.
16. Matsushita O, Tanaka M, Kanki H, et al. Vibrations of rotating machinery. Mathematics for Industry, 2017. 16.
17. Moore JJ, Vannini G, Camatti M et al (2010) Rotordynamic analysis of a large industrial turbocompressor including finite element substructure modeling. *J Eng Gas Turbines Power* 132(8):1233–1243
18. Bajpai A, Vishwakarma P. Finite element analysis of two-crack shaft in a rotor disc-bearing system. 2017.
19. Thompson, Kathryn M. ANSYS mechanical APDL for finite element analysis. 2017.
20. Kumar M S. Rotor Dynamic Analysis Using ANSYS [M]. Springer Netherlands, 2011.
21. Chen X, Liu Y. Finite element modeling and simulation with ANSYS workbench. crc press, 2014.

Publisher's Note Springer Nature remains neutral with regard to jurisdictional claims in published maps and institutional affiliations.